HHS Public Access

Author manuscript

ACS Appl Mater Interfaces. Author manuscript; available in PMC 2019 April 25.

Published in final edited form as:

ACS Appl Mater Interfaces. 2018 April 25; 10(16): 13333–13341. doi:10.1021/acsami.8b01582.

Entanglement-Based Thermoplastic Shape Memory Polymeric Particles with Photothermal Actuation for Biomedical Applications

Qiongyu Guo[a,†,**], **Corey J. Bishop**[a,†,***], **Randall A. Meyer**[a,†], **David R. Wilson**[a], **Lauren Olasov**[b], **Daphne E. Schlesinger**[a], **Patrick T. Mather**[c], **James B. Spicer**[b], **Jennifer H. Elisseeff**[a,b,d,e], and **Jordan J. Green**[a,b,d,e,f,*]

[a]Department of Biomedical Engineering, Institute for Nanobiotechnology, and Translational Tissue Engineering Center, Johns Hopkins University School of Medicine, Baltimore, MD 21231, USA

[b]Department of Materials Science and Engineering, Johns Hopkins University, Baltimore, MD 21218, USA

[c]Department of Chemical Engineering, Bucknell University, Lewisburg, PA 17837, USA

[d]Department of Ophthalmology, Johns Hopkins University School of Medicine, Baltimore, MD 21231, USA

[e]Bloomberg~Kimmel Institute for Cancer Immunotherapy, Johns Hopkins University School of Medicine, Baltimore, MD 21231, USA

[f]Departments of Oncology, Neurosurgery, and Chemical & Biomolecular Engineering, Johns Hopkins University, Baltimore, MD 21231, USA

Abstract

Triggering shape memory functionality under clinical hyperthermia temperatures could enable the control and actuation of shape memory systems in clinical practice. For this purpose, we developed light-inducible shape memory microparticles composed of a poly (D,L-lactic acid) (PDLLA) matrix encapsulating gold nanoparticles (Au@PDLLA hybrid microparticles). This shape memory polymeric system for the first time demonstrates the capability of maintaining an anisotropic shape at body temperature with triggered shape memory effect back to a spherical shape at a narrow temperature range above body temperature with a proper shape recovery speed (37 °C < T < 45 °C). We applied a modified film-stretching processing method with carefully controlled stretching temperature to enable shape memory and anisotropy in these micron-sized

*To whom correspondence should be addressed: green@jhu.edu.

**Present address: Department of Biomedical Engineering, Southern University of Science and Technology, 1088 Xueyuan Rd, Nanshan District, Shenzhen, Guangdong 518055, China

***Present address: Department of Biomedical Engineering, Texas A&M University, Emerging Technologies Building Room 5016 College Station, TX 77843, USA

†These authors contributed equally

SUPPORTING INFORMATION

Characterizations of shape memory particles in terms of various aspects, including SEM characterization of particle morphology, DSC thermal properties, AuNP absorbance spectrum and concentration evaluation in shape memory particles, TEM characterization of pure AuNPs and Au@PDLLA hybrid microparticles, aspect ratio analysis under thermal treatment, shape recovery dynamics as well as macrophage metabolic activity evaluations upon exposure to various doses of shape memory particles.

particles. Accordingly, we achieved purely entanglement-based shape memory response without chemical crosslinks in the miniaturized shape memory system. Furthermore, these shape memory microparticles exhibited light-induced spatiotemporal control of their shape recovery using a laser to trigger photothermal heating of doped gold nanoparticles. This shape memory system is composed of biocompatible components and exhibits spatiotemporal controllability of its properties, demonstrating potential for various biomedical applications, such as tuning macrophage phagocytosis as demonstrated in this study.

Graphical Abstract

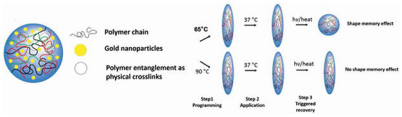

Keywords

Thermoplastic; Polymer, Gold; Nanoparticle; Anisotropy; Shape; Photothermal; Shape Memory

1. INTRODUCTION

Entropy elasticity has been widely applied to empower polymers with shape-memory functionality for various applications such as actuators, sensors and biomedical applications.[1–3] Shape memory polymers (SMPs) can exhibit an entropy-driven shape memory effect (SME) through recovering from a temporary, deformed shape at a low entropy state to a permanent, equilibrium shape at an entropically more favorable state by an external stimulus.[4] The application of SMPs for therapeutic purposes, however, has been dampened by the lack of controllability of SME under restrictive clinical requirements. Most SMPs can be thermally induced to undergo SME through an external application of heat or other actuation methods such as light, microwave or magnetic field.[5–7] Generally these materials are deformed under a mechanical stress and then triggered to revert back to their original form through bulk heating past the transition temperature (T_t) of the material.[8] Clinical hyperthermia treatments are performed at a maximum of 45 °C for less than 30 min to prevent thermal injury and significant cell death.[9] Maintaining SMP shapes at 37 °C but only triggering SME at a narrow temperature range (37 °C < T < 45 °C) with a proper speed for clinical applications has been extremely challenging. Although SMPs with transition temperatures near body temperature have been reported, no systems presented controllability under clinical hyperthermia conditions at a suitable speed.[10–14] As a result, the development of an SMP platform with a T_t in the optimal biocompatible range and the ability to be rapidly controlled in shapes is highly desirable to analyze the potential application of SME in biomedical therapeutics.

The development of shape memory polymeric systems down to micron/submicron scales had been challenging until a film-stretching method recently enabled the facile programming of shape-memory functionality at such small scales.[15–20] Most often SMPs of small sizes require either chemical crosslinks[21] or an additional set of polymer domains serving as physical netpoints[22] that determine the permanent shape of the material. Polymer

entanglements, a universal property of polymers with sufficient molecular weight, can also act as efficient physical netpoints.[5,23] On the macroscale, entanglement-based shape memory has been well-recognized and used industrially to produce shrink films. For a typical use, commercial goods are loosely wrapped with a biaxially stretched plastic film that is subsequently heated to relax the film to a smaller unoriented size that can provide a close-fitting, high clarity wrapping.[24] The use of polymer entanglements can potentially open a door for a broader selection of thermoplastic polymers in shape memory systems for a variety of applications such as biomedical applications with restrictive requirements in chemistry or materials modification.[25] Yet no study to date has successfully implemented such a strategy in miniature shape memory systems probably due to processing and handling difficulties.

One therapeutic application that could benefit from small-scale SMPs is the use of micro- and nanoparticles for drug delivery. Recently, there has been great interest in the use of non-spherical micro-/nanoparticles for drug delivery applications.[26,27] This is due to two beneficial properties exhibited by non-spherical shaped compared to spherical shaped particles. The first is reduced non-specific cellular uptake. This has been found to be linked to the interaction of the particle with the cell membrane, namely the angle of approach.[15] It has been repeatedly demonstrated that non-spherical ellipsoidal micro- and nanoparticles can avoid cellular uptake and phagocytosis compared to their spherical counterparts.[16,28] The second advantageous property is the feature of increased targeted binding. This is mediated by the increased surface area and radius of curvature available for interaction with biological surfaces.[29] This feature was exploited to direct the targeted accumulation of nanoparticles in the lung and brain endothelium compared to spherical particles.[18] Furthermore, it has been found that the increased targeted binding of non-spherical artificial antigen presenting cells to T-Cells enhances the activity of the particles for immunomodulation.[30] Reversion of an ellipsoidal to a spherical microparticle has been shown to increase the phagocytic rate by macrophages, but this particular material took hours to undergo a surface-tension driven shape switch instead of entropy-driven shape memory response with controls in the shapes at specific temperatures.[17]

There is a need for new biomedical systems that can exhibit externally triggered changes to their physical and biological properties in a spatiotemporally controlled manner. One strategy to enable spatiotemporal control over SME is through the use of a photothermal converter such as gold nanoparticles (AuNPs).[31] AuNPs have been utilized in a wide variety of applications including image contrast,[32] gene therapy (for co-delivery of DNA/siRNA[33] and to assert control over expression kinetics[34]), and photothermal treatment of tumors[35]. Typically, the photothermal heating process happens when free electrons of AuNPs are photo-excited via surface plasmon resonance and release their energy first through electron-phonon interactions to the gold lattice inside the AuNPs and then through phonon-phonon interactions to the surrounding medium.[36–38] Zhao et al.[31,39,40] and other groups[41–43] have recently reported that, although gold does not exhibit SME, it could be distributed in colloidal form throughout an SMP for photothermal conversion, to couple the spatiotemporally precise application of laser energy to trigger SME. Nevertheless, it was unclear if such a AuNP-based photothermal trigger could be applied to SMP in small scales. In this study, we hypothesized that the AuNPs embedded in shape memory particles could

be plasmonically heated under continuous wave laser irradiation and then transfer their thermal energy to their surrounding PDLLA matrix, which could subsequently result in a shape memory response of the particles when the temperature of the PDLLA matrix increased beyond T_t. The main objective of this study was to develop a micron-scale biocompatible shape memory system with both an optimal T_t within the human body-tolerable temperature range and a spatiotemporally controlled trigger for induction of SME for biomedical applications.

2. RESULTS AND DISCUSSION

2.1. Fabrication and Characterizations of Shape Memory Microparticles.

We developed a shape memory micro-system based on high molecular weight purely amorphous polymer, i.e. poly(D,L-lactic acid) (PDLLA), which was expected to only have polymer entanglements serving as physical netpoints for shape memory actuation. Recently, Petisco-Ferrero et al. systematically tested the rheological properties of PDLLA of multiple molecular weights and observed the rubbery plateau of the material that confirms the entanglements of the polymer with an entanglement molecular weight of 5200 g/mol.[44] We purposely applied this widely used biocompatible polymer without any chemical modifications in our shape memory system because of its having already been proved safety to human body for clinical translation.[25] This shape memory system encapsulated a hydrophobically stabilized AuNP formulation as a photothermal trigger. The material and its application are summarized in Figure 1a. PDLLA microparticles encapsulating AuNP (Dia. 14 ± 6 nm) for photothermal conversion were synthesized by bulk emulsion. Particles fabricated by bulk emulsion with polymers of significantly high molecular weight are expected to have entanglements serving as efficient physical crosslinks that entropically drive SME.[2,5] We then imparted a deforming stress on the microparticles through use of an automated thin film stretching method.[20] The spherical and non-spherical microparticles were characterized by scanning electron microscopy (Figure S1a–b) (Dia. of the microspheres: 5.22 μm +/− 1.39 μm, Figure S1c). The PDLLA we selected was amorphous thermoplastic polymer showing a glass transition temperature (T_g) of 41.3 °C in the particles (Figure S2). Note that the breadth of glass transition of PDLLA was 9 °C starting from 39 °C to 48 °C, which is right above the body temperature of 37 °C. We hypothesized that the glass transition could be employed to trigger SME in PDLLA particles.

Through stretching at low temperatures (e.g. 65 °C) we expected the physical crosslinks to remain intact and drive the SME upon heating past the transition temperature. On the other hand, we hypothesized that stretching at high temperatures (e.g. 90 °C) would erase this polymer entanglement and thus the SME. To confirm the presence of polymer alignment and the entropy driven mechanism of the SME, microparticles stretched at either 65 °C or 90 °C were analyzed by polarized light optical microscopy (POM) (Figure 1b). As shown in the images, the particles stretched at 65 °C showed strong birefringence under crossed polarizers, indicating polymer alignment inside the particles. In contrast, the particles stretched at 90 °C only exhibited light reflection from the particle surface, suggesting random orientation of polymer chains. This confirmed our theory that low temperatures

would preserve the polymer entanglements of the particles whereas high temperatures would erase them.

As part of the characterization process we evaluated the properties of the colloidal gold immobilized in the polymer matrix. UV-Vis spectroscopy indicated that the AuNPs maintained their absorption peak at 530 nm even after encapsulation (Figure S3a). We calculated the concentration of nanoparticles through analysis of absorbance and were able to derive a standard curve of gold nanoparticle concentration vs. absorbance (Figure S3b). Using this standard we determined the concentration of the gold in the microparticles to be 1.63×10^{10} AuNPs per mg of loaded PDLLA microparticles. We further characterized the gold content of the microparticles through transmission electron microscopy (TEM) (Figure S4). There was approximately 0.58 ng of AuNPs per mg of PDLLA. Each AuNP and PDLLA microparticle had a mass of approximately 25 attograms ($x10^{-18}$) and 98 pg, respectively, constituting approximately 0.041% of AuNPs by mass. Each PDLLA microparticle contained approximately 1.6×10^{3} AuNPs. The lower magnification images (Figure S5a–b) were unable to distinguish AuNP encapsulation compared to PDLLA microparticles without AuNPs (Figure S6) which were used to prepare the UV-Vis standard curve (Figure S3b). However, the higher magnification images made it possible to identify individual AuNPs in the microparticles (Figure S5c–d, red arrows). As expected, the diameters of the encapsulated AuNPs within the PDLLA microparticles were not as apparent and difficult to distinguish in comparison to Figure S4 which lead to a slight increase in the calculated diameters from 14 ± 6 nm (Figure S4) to 15 ± 3 nm (Figure S5a–b) via ImageJ (Fiji). These experiments confirmed that we could successfully encapsulate absorptive colloidal gold at high concentrations in our particles without significant aggregation.

2.2. Direct Thermal Actuation of Shape Memory Microparticles.

Upon successful synthesis and characterization of the shape memory materials, we next turned to analyze the entropy-driven SME property of the particles. We first assessed the SME through bulk heating of the media to determine the window of trigger temperatures before the surface tension effects drive the particles back to spheres. As illustrated by aspect ratio analysis vs. time (Figure S7) for different bulk heating temperatures, the low temperature stretched particles maintained their shapes at 37 °C over 24 h and completely recovered their shapes at all temperatures tested above 37 °C (i.e. 40 °C, 45 °C, and 50 °C) within 30 min. Therefore, these particles could rapidly undergo SME even at a temperature slightly below T_g (i.e. 41.3 °C). This can be explained by the small-sized shape memory system in micron scale and the shape recovery temperature still above the initiation temperature of glass transition (i.e. 39 °C). Furthermore, we observed that the birefringence of these particles gradually decreased with time during shape recovery process (supplementary Movie S10), which confirms our hypothesis of polymer alignment as the driving force for SME. However, the high temperature stretched particles did not begin to revert until longer incubations at 45 °C and 50 °C. This provided us with an optimal transition temperature range for entropy-driven shape memory that is within the biocompatible temperature range. Of note, while the high temperature stretched particles not showing a shape memory effect could naturally deform back to spheres over longer time

scales of days due to surface tension, the particles showing a shape memory effect remarkably increased the shape recovery rate at a relevant switch-like speed within the body-compatible temperature range. This shape change to the thermodynamically favored sphere obviates challenges with fixity and recovery that are typically present in macroscopic shape memory systems.

2.3. Photothermal Actuation of Shape Memory Microparticles.

With verification of the predicted SME in a bulk heating scenario, we then evaluated the capability for the laser to trigger the shape memory effect through photothermal heating of the gold laden microparticles in bulk media. In order to verify entropy driven SME, we compared the 65 °C low temperature stretched and the 90 °C high temperature stretched microparticles for analysis of SME by photothermal heating. We irradiated the particles for 1–5 min using the 532 nm laser at 2 W focused on a circular spot, 5 mm in diameter (Figure 2a–h). As shown in the SEM images of the irradiated particles, the low temperature stretched particles underwent visibly significant SME within 3 min of the start of laser irradiation (Figure 2a–d). However, there was almost no shape change or SME observed in the high temperature stretched particles for that same time period as well as throughout the entire 5 min experiment (Figure 2e–h). We further characterized this SME through aspect ratio analysis of the irradiated particles. As shown in Figure 2i, the low temperature stretched particles showed near complete reversion to an aspect ratio of 1 (spherical), whereas the high temperature stretched particles maintained a high aspect ratio (>3) throughout the duration of the heating. Following a percent reversion normalization equation we determined that the low temperature particles reverted nearly 100% back to their spherical form whereas the high temperature stretched particles showed approximately 10–20% reversion over the duration of the experiment (Figure 2j). In order to verify this difference was not due to differential photothermal heating of the particles stretched at different temperatures, we tracked the bulk media temperature during the experiment and found the temperatures for the two particle sets to be identical with respect to time of irradiation (Figure 2k).

2.4. Spatiotemporal Control of Shape Memory Recovery.

Upon verification that the SME could be triggered by photothermal heating, we then sought to characterize the spatial resolution of the SME with respect to the laser irradiation spot. To accomplish this goal, we formulated the gold laden microparticles with a fluorophore, stretched them at a low temperature, and immobilized them in an artificial extracellular matrix made of a poly(ethylene glycol) (PEG) hydrogel. The gel was subsequently irradiated and determined to undergo successful heating based on IR imaging of the matrix (Figure 3a). After irradiation for 5 min, we imaged the gel under confocal microscopy to analyze the aspect ratio of the particles with respect to the spatial dimension. We found that the region of the gel directly irradiated with the laser successfully exhibited SME as evidenced by reversion back to spherical form (Figure 3b). Immediately outside of the irradiation region, there was partial SME observed in a 1 mm region on either side, however the reversion to spherical form was not complete most likely suggesting this was the result of the thermal conductivity of the matrix. Outside of this small 1 mm region, there was little or no SME observed suggesting the laser spot size specifies the spatial resolution of the SME. This is

also illustrated in Figure 3c. As shown in these confocal micrographs, there was a clear visual transition from the region that was not irradiated (yielding only high aspect ratio particles) and the region that was irradiated (yielding only spherical particles). This confirms that not only is the SME able to be triggered by a laser in the biocompatible temperature range, but also the SME is restricted (with 1 mm resolution) to the irradiated area of the laser.

2.5. Shape Memory Response Impacts Macrophage Phagocytosis.

One of the advantageous properties of an anisotropic over a spherical equivalent is that due to the entropic interaction of the particle with the cell membrane, there is less non-specific endocytosis and phagocytosis of ellipsoidal particles compared to spherical particles and hence, slower elimination from the body.[28] This was recently exploited in shape-switching particles that are triggered to revert back to spherical form to enable more rapid phagocytosis of the particles.[17] We wanted to determine if the thermally triggered SME in the gold laden microparticles could render the particles more susceptible to phagocytosis by macrophages. To confirm that SME could be observed in the fluorophore loaded particles, we did confocal imaging of bulk heated particles stretched at either low or high temperatures to confirm SME. As shown in Figure 4a–b, the low temperature stretched particles exhibited complete reversion to spherical form whereas the high temperature stretched particles had no reversion (for full time course, see Figure S8). Upon addition of the particles to the macrophages, we triggered the SME through short term (15 min) bulk heating of the cells to 45 °C. As shown in the confocal micrographs of cells with low temperature stretched particles, this heating resulted in spherical particles that could be more readily phagocytosed than the ellipsoidal high temperature stretched particles (Figure 4c–d). This was quantitatively assessed using flow cytometry to determine the percent uptake of the particles (Figure 4e) and the geometric fluorescent signal mean for comparison of how many particles were taken up per cell (Figure 4f). As shown, there was statistically significant reduction in both the percent uptake positive and geometric mean for high temperature stretched, ellipsoidal microparticles compared to the SME triggered low temperature stretched particles. Both bulk heated and laser triggered shape memory microparticles demonstrated similar effect in controlling macrophage response. This observed trend was significant for a variety of doses ranging from 3.75 – 25 μg particles/30,000 cells. We also assessed the viability of the macrophages to determine if the particles exerted any toxicity on the cells. As shown in Figure S9, the viability was unaltered over a wide range of doses compared to a no treatment control.

3. CONCLUSIONS

In this study, we have developed a novel shape memory system with entropy-driven SME that can be triggered at biocompatible temperatures in a spatiotemporally controlled manner. To our knowledge, this is the first instance of a material bearing all of these properties and this biotechnology could enable biomedical applications ranging from precise triggered drug delivery to switchable biomedical microdevices. We have verified that these particles possess physical polymeric alignment, driving the entropy based SME. The particles can be triggered to change shape upon irradiation and photothermal heating of encapsulated

AuNPs. This triggering is both specific to the spot of irradiation, and the time of irradiation thus establishing spatiotemporal control over the SME. Furthermore, this material exhibits SME when the bulk media temperature is 40 °C. This is significantly below temperatures at which thermal injury occurs, rendering these particles biocompatible. This technology and related platforms can enable the once elusive union of shape memory materials and biomedical applications.

4. EXPERIMENTAL SECTION

4.1. Hydrophobic Gold Nanoparticle Synthesis.

A modified version of Chatterjee et al.[9] was used to synthesize hydrophobic gold nanoparticles. More specifically, lyophilized 1,2-Dioleoyl-sn-glycero-3-phosphocholine (Avanti® Polar Lipids; DOPC) was reconstituted at 25 mg/mL in chloroform and mixed with toluene, forming a 250 μg/mL solution (33 mL) which was vortexed for about 10 seconds. 5 mL of this solution put into 6 different 20 mL scintillation vials (underlying metal cap insert was extracted and discarded out of each cap to not reduce Au^{3+}. Tetrachloroauric acid trihydrate ($HAuCl_4$) was reconstituted in ultrapure distilled water to 100 mg/mL and served as a stock. 250 μL of the stock $HAuCl_4$ solution was mixed with 24.75 mL of ultra-pure distilled water forming a 1 mg/mL solution of $HAuCl_4$. 2 mL of this 1 mg/mL solution was added to each of the 6 20 mL scintillation vials already containing 5 mL of the 250 μg/mL DOPC solution in toluene. Each vial also contained a VWR magnetic stir bar. Prior to placing the scintillation vials on a multi-position stir plate, each vial was vortexed to produce a non-transparent, and to the extent possible, a homogenous mixture of the aqueous and organic phases prior to adding 1 mL of sodium citrate tribasic dihydrate at 10 mg/mL drop-wise. The stirring was continued for approximately 18 hours. Once completed, the organic and aqueous phases were allowed to sufficiently separate over a few minutes and the organic toluene phases were extracted, mixed, and placed into a new scintillation vial. All aqueous solvent was again taken out of the organic phase if phase separation occurred.

To encapsulate the lipid-coated gold nanoparticles into the PDLLA microparticles, the gold nanoparticles (1 mL of gold nanoparticles in toluene in 1.5 mL tubes; total of 5 mL) were centrifuged at 16,000 rcf. All but the pellets were aspirated (975 μL) and replaced with an equal volume of dichloromethane (DCM). The gold nanoparticles were sonicated (Misonix) to become a homogenous mixture in the DCM. The 5 mL of gold nanoparticles in DCM were used directly in the single-emulsion encapsulation during PDLLA microparticle formation.

4.2. PDLLA Anisotropic Microparticle Synthesis and Characterization.

PDLLA with ester endcap (Mn = 70.2 kDa, PDI = 1.95) was purchased from PolySciTech (Akina Inc.). A larger molecular weight polydispersity is helpful to better entangle polymer chains and contribute to the shape memory effect. Two solutions of polyvinyl alcohol were made (PVA1 = 1% PVA; PVA0.5 = 0.5% PVA) in deionized MilliQ water. 200 mL of PVA0.5 was dispensed into a beaker with a VWR stir bar (spinning at 450 RPM). 100 mg of PDLLA was dissolved in 5 mL of DCM containing gold nanoparticles and poured into 50 mL of PVA1 while being homogenized (5000 RPM). For fluorescent visualization of the

particles, 1 mg of Nile Red or 7-amino-4-methyl coumarin was added to the DCM mixture. The microparticle solution encapsulating gold nanoparticles was poured into the stirring PVA0.5 and stirred for an additional 4 hours to evaporate the organic solvent. Subsequently, we washed the microparticles 3x by centrifugation at 4 °C (3000 rcf; 5 minutes) to remove PVA. After the 3rd wash, the microparticles were resuspended in 1 mL of deionized water, triturated to avoid clumping, snap frozen in liquid nitrogen, lyophilized, and then stored dry at 4 °C or below until further use.

The particles were deformed into anisotropic shapes by an automated thin film stretching procedure as described in Meyer et. al.[20] Briefly, the particles were lyophilized, suspended in a solution containing 10% w/w PVA and 2% w/w glycerol, and then cast into a PVA film. The film was allowed to dry overnight and mounted on customized aluminum blocks. After 10 min of heating at a predetermined temperature, the film was loaded for 1-D stretching with stepper motors set at a strain rate of 0.2 min^{-1}. The stretched film was immediately cooled at room temperature for one hour, cut from the grips, and dissolved in water. The resulting particle suspension was then washed 3 times and lyophilized prior to use.

To characterize the microparticle size and shape, scanning electron microscopy was utilized. Lyophilized particle samples were spread onto carbon tape mounted to aluminum tacks. The particles were then sputter coated with 30 nm of a gold-chromium alloy and imaged with a LeoFESEM. Size was determined by ImageJ analysis of the resulting SEM micrographs. Aspect ratio throughout all of the studies was determined through analysis of the particles and taking the ratio of the longer axis to the shorter axis. For the fluorescent particle image analysis, confocal imaging was completed using a Zeiss 780 FCS confocal microscope.

Differential scanning calorimetry (DSC) was carried out using a DSC 8000 (Perkin Elmer, Waltham, MA) to determine the glass transition of PDLLA particles. The particles incubated in water was sealed in an aluminum pan. The DSC tests were performed by heating-cooling-heating between 10 °C and 90 °C at 10 °C/min. The second heating trace was analyzed by Pyris Series software (Perkin Elmer) to determine the glass transition temperature and glass transition breadth.

Polarized light optical microscopy (POM) was utilized to monitor polymer alignment in stretched microparticles. POM studies were performed in an Olympus BX51 microscope equipped with 90° crossed polarizers, a HCS402 hot stage (Instec Inc.) and a CCD camera (QImaging). Images were acquired using QCapture Pro software (QImaging) at various angles of the sample stage (i.e. 0°, 45°, 90°, 135°, 180°, 225°, 270° and 315°). Shape recovery of 65 °C stretched microparticles was monitored in the hot stage set at 45 °C.

4.3. Characterization of Gold Nanoparticles in PDLLA Microparticles.

In order to quantify the number of AuNPs within the microparticles, a standard curve was created; the AuNPs' stock concentration was assessed using Beer-Lambert's law[45] using an extinction coefficient of 3.189×10^{10} M^{-1} cm^{-1}. A standard curve was created using various dilutions of the AuNPs in toluene (1 mL) with 5 mg of pure PDLLA microparticles solvated in 400 μL of dimethyl sulfoxide (DMSO); 1 μL of the total volume of 1400 μL was used to assess the absorbance via NanoDrop (Thermo Scientific) (Figure S3). When quantifying

how many AuNPs there were per mg of particle, 5 mg of 4 unknown samples were solvated in 1 mL of toluene and 400 μL of DMSO. The number of AuNPs/μL of sample was interpolated with the standard curve and multiplied by 1400 (total volume in μL) and divided by 5 mg.

4.4. Laser Triggering of Shape Memory Effect.

For analysis of the temporal control of the shape memory effect, the particles were irradiated with a 532 nm laser at a power of 2 W distributed across a 5 mm diameter circular spot. The particles were irradiated at a concentration of $4*10^7$ particles/mL in a glass cuvette. Temperature was assesed with a Fluke thermocoupling device. After irradiation for the indicated period of time in the experiment, the particles were collected and imaged under SEM for evaluation of aspect ratio. The measured aspect ratio (AR_m) was then normalized to the initial aspect ratio (AR_o) to give percent shape reverison accoding to the following formula:

$$\frac{\left(AR_m - AR_o\right)}{1 - AR_o} \times 100\%$$

Characterization of the spatial selectivity of the shape memory effect was achieved through immobilization of the particles in a PEG hydrogel at a concentration of 2×10^5 particles/mL PEG gel. The hydrogel was then mounted to the laser and irradiated at a single circular spot approximately 5 mm in diameter for 5 minutes. Heating of PEG hydrogel was tracked by imaging with an FL-IR camera. After laser irradiation, the gel was imaged under confocal microscopy and individual images 200 μm in width were generated and stiched together for the length of the hydrogel. Aspect ratio was then quantified across the image to analyze the spatial dependence of the shape memory effect on the laser spot size.

4.5. Cell Uptake Experiments.

Cell uptake of the particles triggered to undergo the shape memory effect was assessed using RAW 264.7 macrophages. Cell uptake was evaluated using flow cytometry and confocal microscopy. For flow cytometry, the cells were seeded onto a 96-well plate at a density of 30,000 cells/well two days prior to the start of the experiment. On the day of the experiment, the medium was aspirated, and medium containing the particles at the indicated dose was added. Following an incubation of 4 hours at 37 °C the cells were washed 3 times with 1x PBS and prepared for flow cytometry or confocal microscopy. For distinction of particles from cells, cells were then stained with carboxyfluorescein succinyl ester (CFSE) according to the manufacturers protcol. CFSE stained cells were then removed from the plate with vigrous trituration and were analyzed by flow cytometry. Flow cytometry was performed using a BD Accuri C6 (BD Biosciences, San Jose, CA) flow cytometer with two lasers (488 and 633 nm) with four channels corresponding to green, yellow, red and far-red fluorescence (FL1 at 530±15 nm, FL2 at 565±10 nm, FL3 at 610±10 nm, and FL4 at 675±12.5 nm respectively) in combination with a Hypercyt autosampler (Intellicyt, Albuquerque, NM).

For confocal microscopy, the cells were cultured on a LabTek chamber slide at a density of 30,000 cells per well. After 4 hours incubation time with the particles, the excess particles

were washed away with 3 washes of 1x PBS and then the cells were fixed with 10% formalin for 15 minutes at room temperature. Following fixation and washing, the cells were stained with Alexa 647 phalloidin for actin visualization and DAPI for nuclear visualization following manufacturer protocols. The cells were then imaged using a Zeiss FCS 780 confocal microscope. Cell viability was evaluated using an MTS Celltiter 96 Aqueous One (Promegra, Madison, WI) cell proliferation assay following the manufacturer's protocol.

Supplementary Material

Refer to Web version on PubMed Central for supplementary material.

ACKNOWLEDGMENTS

Dr. Q. Guo, Dr. C. J. Bishop, and R. A. Meyer contributed equally to this work. The authors thank the JHU-Coulter Translational Partnership, the TEDCO Maryland Innovation Initiative, the Bloomberg~Kimmel Institute for Cancer Immunotherapy, and the NIH (R01-EB016721 and P30-EY001765). R. A. Meyer thanks the NIH Cancer Nanotechnology Training Center (R25CA153952) at the JHU Institute for Nanobiotechnology and the Achievement Rewards for College Scientists (ARCS) and the National Cancer Institute of the NIH (F31CA214147) for fellowship support.

REFERENCES

(1). Behl M; Razzaq MY; Lendlein A Multifunctional Shape-Memory Polymers. Adv. Mater 2010, 22, 3388–3410. [PubMed: 20574951]

(2). Hager MD; Bode S; Weber C; Schubert US Shape Memory Polymers: Past, Present and Future Developments. Prog. Polym. Sci 2015, 49–50, 3–33.

(3). Chan BQ; Low ZW; Heng SJ; Chan SY; Owh C; Loh XJ Recent Advances in Shape Memory Soft Materials for Biomedical Applications. ACS Appl. Mater. Interfaces 2016, 8, 10070–10087. [PubMed: 27018814]

(4). Lendlein A; Kelch S Shape-Memory Polymers. Angew. Chem. Int. Ed 2002, 41, 2034–2057.

(5). Zhao Q; Qi HJ; Xie T Recent Progress in Shape Memory Polymer: New Behavior, Enabling Materials, and Mechanistic Understanding. Prog. Polym. Sci 2015, 49–50, 79–120.

(6). Wischke C; Neffe AT; Steuer S; Lendlein A Evaluation of a Degradable Shape-Memory Polymer Network as Matrix for Controlled Drug Release. J. of Control. Release 2009, 138, 243–250. [PubMed: 19470395]

(7). Wang WX; Liu YJ; Leng JS Recent Developments in Shape Memory Polymer Nanocomposites: Actuation Methods and Mechanisms. Coordin. Chem. Rev 2016, 320, 38–52.

(8). Mather PT; Luo XF; Rousseau IA Shape Memory Polymer Research. Annu. Rev. Mater. Res 2009, 39, 445–471.

(9). Chatterjee DK; Diagaradjane P; Krishnan S Nanoparticle-Mediated Hyperthermia in Cancer Therapy. Ther. Deliv 2011, 2, 1001–1014. [PubMed: 22506095]

(10). Le DM; Kulangara K; Adler AF; Leong KW; Ashby VS Dynamic Topographical Control of Mesenchymal Stem Cells by Culture on Responsive Poly(Epsilon-Caprolactone) Surfaces. Adv. Mater 2011, 23, 3278–3283. [PubMed: 21626577]

(11). Davis KA; Burke KA; Mather PT; Henderson JH Dynamic Cell Behavior on Shape Memory Polymer Substrates. Biomaterials 2011, 32, 2285–2293. [PubMed: 21224032]

(12). Hearon K; Wierzbicki MA; Nash LD; Landsman TL; Laramy C; Lonnecker AT; Gibbons MC; Ur S; Cardinal KO; Wilson TS; Wooley KL; Maitland DJ A Processable Shape Memory Polymer System for Biomedical Applications. Adv. Healthcare Mater 2015, 4, 1386–1398.

(13). Baker RM; Tseng LF; Iannolo MT; Oest ME; Henderson JH Self-Deploying Shape Memory Polymer Scaffolds for Grafting and Stabilizing Complex Bone Defects: A Mouse Femoral Segmental Defect Study. Biomaterials 2016, 76, 388–398. [PubMed: 26561935]

(14). Zhang Y; Gao H; Wang H; Xu Z; Chen X; Liu B; Shi Y; Lu Y; Wen L; Li Y; Li Z; Men Y; Feng X; Liu W Radiopaque Highly Stiff and Tough Shape Memory Hydrogel Microcoils for Permanent Embolization of Arteries. Adv. Funct. Mater 2018, 1705962.

(15). Champion JA; Mitragotri S Role of Target Geometry in Phagocytosis. Proc. Natl. Acad. Sci. U. S. A 2006, 103, 4930–4934. [PubMed: 16549762]

(16). Sharma G; Valenta DT; Altman Y; Harvey S; Xie H; Mitragotri S; Smith JW Polymer Particle Shape Independently Influences Binding and Internalization by Macrophages. J. Control. Release 2010, 147, 408–412. [PubMed: 20691741]

(17). Yoo JW; Mitragotri S Polymer Particles That Switch Shape in Response to a Stimulus. Proc. Natl. Acad. Sci. U.S.A 2010, 107, 11205–11210. [PubMed: 20547873]

(18). Kolhar P; Anselmo AC; Gupta V; Pant K; Prabhakarpandian B; Ruoslahti E; Mitragotri S Using Shape Effects to Target Antibody-Coated Nanoparticles to Lung and Brain Endothelium. Proc. Natl. Acad. Sci. U.S.A 2013, 110, 10753–10758. [PubMed: 23754411]

(19). Ho CC; Keller A; Odell JA; Ottewill RH Preparation of Monodisperse Ellipsoidal Polystyrene Particles. Colloid Polym. Sci 1993, 271, 469–479.

(20). Meyer RA; Meyer RS; Green JJ An Automated Multidimensional Thin Film Stretching Device for the Generation of Anisotropic Polymeric Micro - and Nanoparticles. J. Biomed. Mater. Res. A 2015, 103, 2747–2757. [PubMed: 25641799]

(21). Brosnan SM; Jackson AMS; Wang YP; Ashby VS Shape Memory Particles Capable of Controlled Geometric and Chemical Asymmetry Made from Aliphatic Polyesters. Macromol. Rapid Comm 2014, 35, 1653–1660.

(22). Wischke C; Schossig M; Lendlein A Shape-Memory Effect of Micro-/Nanoparticles from Thermoplastic Multiblock Copolymers. Small 2014, 10, 83–87. [PubMed: 23847123]

(23). Gu XZ; Mather PT Entanglement-Based Shape Memory Polyurethanes: Synthesis and Characterization. Polymer 2012, 53, 5924–5934.

(24). Butler TI; Morris BA In Multilayer Flexible Packaging: Technology and Applications for the Food, Personal Care, and over-the-Counter Pharmaceutical Industries; Wagner JR, Ed; William Andrew: Burlington, MA, 2010; Chapter 15, pp 205–230.

(25). Doppalapudi S; Jain A; Khan W; Domb AJ Biodegradable Polymers-an Overview. Polym. Advan. Technol 2014, 25, 427–435.

(26). Meyer RA; Green JJ Shaping the Future of Nanomedicine: Anisotropy in Polymeric Nanoparticle Design. Wiley Interdiscip. Rev. Nanomed. Nanobiotechnol 2016, 8, 191–207. [PubMed: 25981390]

(27). Meyer RA; Sunshine JC; Green JJ Biomimetic Particles as Therapeutics. Trends Biotechnol. 2015, 33, 514–524. [PubMed: 26277289]

(28). Meyer RA; Sunshine JC; Perica K; Kosmides AK; Aje K; Schneck JP; Green JJ Biodegradable Nanoellipsoidal Artificial Antigen Presenting Cells for Antigen Specific T-Cell Activation. Small 2015, 11, 1519–1525. [PubMed: 25641795]

(29). Toy R; Peiris PM; Ghaghada KB; Karathanasis E Shaping Cancer Nanomedicine: The Effect of Particle Shape on the in Vivo Journey of Nanoparticles. Nanomedicine 2014, 9, 121–134. [PubMed: 24354814]

(30). Sunshine JC; Perica K; Schneck JP; Green JJ Particle Shape Dependence of Cd8+ T Cell Activation by Artificial Antigen Presenting Cells. Biomaterials 2014, 35, 269–277. [PubMed: 24099710]

(31). Zhang H; Zhao Y Polymers with Dual Light-Triggered Functions of Shape Memory and Healing Using Gold Nanoparticles. ACS Appl. Mater. Interfaces 2013, 5, 13069–13075. [PubMed: 24308556]

(32). Mieszawska AJ; Mulder WJ; Fayad ZA; Cormode DP Multifunctional Gold Nanoparticles for Diagnosis and Therapy of Disease. Mol. Pharm 2013, 10, 831–847. [PubMed: 23360440]

(33). Bishop CJ; Tzeng SY; Green JJ Degradable Polymer-Coated Gold Nanoparticles for Co-Delivery of DNA and Sirna. Acta Biomater. 2015, 11, 393–403. [PubMed: 25246314]

(34). Bishop CJ; Liu AL; Lee DS; Murdock RJ; Green JJ Layer-by-Layer Inorganic/Polymeric Nanoparticles for Kinetically Controlled Multi-Gene Delivery. J. Biomed. Mater. Res. A 2016, 104A, 707–713.

(35). Terentyuk G; Panfilova E; Khanadeev V; Chumakov D; Genina E; Bashkatov A; Tuchin V; Bucharskaya A; Maslyakova G; Khlebtsov N; Khlebtsov B Gold Nanorods with a Hematoporphyrin-Loaded Silica Shell for Dual-Modality Photodynamic and Photothermal Treatment of Tumors in Vivo. Nano Res. 2014, 7, 325–337.

(36). Huang XH; Jain PK; El-Sayed IH; El-Sayed MA Plasmonic Photothermal Therapy (Pptt) Using Gold Nanoparticles. Laser Med. Sci 2008, 23, 217–228.

(37). Abadeer NS; Murphy CJ Recent Progress in Cancer Thermal Therapy Using Gold Nanoparticles. J. Phys. Chem. C 2016, 120, 4691–4716.

(38). Riley RS; Day ES Gold Nanoparticle-Mediated Photothermal Therapy: Applications and Opportunities for Multimodal Cancer Treatment. Wires Nanomed. Nanobi 2017, 9.

(39). Zhang HJ; Xia HS; Zhao Y Optically Triggered and Spatially Controllable Shape-Memory Polymer-Gold Nanoparticle Composite Materials. J. Mater. Chem 2012, 22, 845–849.

(40). Zhang HJ; Zhang JM; Tong X; Ma DL; Zhao Y Light Polarization-Controlled Shape-Memory Polymer/Gold Nanorod Composite. Macromol. Rapid Comm 2013, 34, 1575–1579.

(41). Xiao ZW; Wu Q; Luo SD; Zhang C; Baur J; Justice R; Liu T Shape Matters: A Gold Nanoparticle Enabled Shape Memory Polymer Triggered by Laser Irradiation. Part. Part. Syst. Char 2013, 30, 338–345.

(42). Leonardi AB; Puig J; Antonacci J; Arenas GF; Zucchi IA; Hoppe CE; Reven L; Zhu L; Toader V; Williams RJJ Remote Activation by Green-Light Irradiation of Shape Memory Epoxies Containing Gold Nanoparticles. Eur. Polym. J 2015, 71, 451–460.

(43). Zheng YW; Li J; Lee E; Yang S Light-Induced Shape Recovery of Deformed Shape Memory Polymer Micropillar Arrays with Gold Nanorods. RSC Adv. 2015, 5, 30495–30499.

(44). Petisco-Ferrero S; Fernandez J; San Martin MMF; Ibarburu PAS; Oiz JRS The Relevance of Molecular Weight in the Design of Amorphous Biodegradable Polymers with Optimized Shape Memory Effect. J. Mech. Behav. Biomed 2016, 61, 541–553.

(45). Liu X; Atwater M; Wang J; Huo Q Colloids Surf. B Biointerfaces 2007, 58, 3. [PubMed: 16997536]

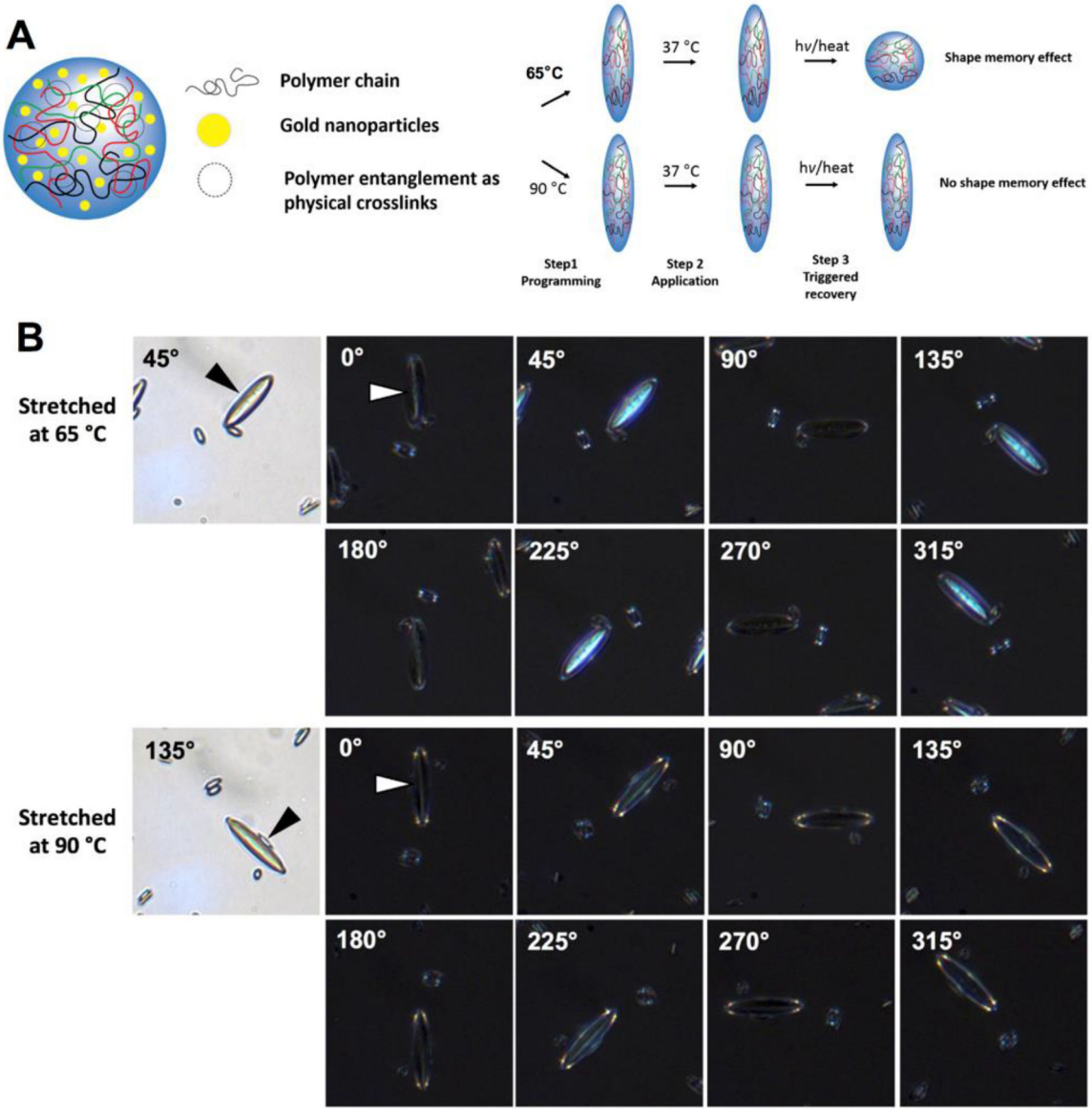

Figure 1.

Polymeric particle entropy-driven shape memory effect. (A) Poly (D,L lactic acid) particles were fabricated encapsulating hydrophobic lipid stabilized gold nanoparticles. Due to high molecular weight of the polymer in use, physical crosslinks of the polymer were present in the sample. Polymeric particles are stretched to anisotropic shapes under low or high temperatures and then the entropy driven shape memory effect was triggered by thermal means. Low temperature stretched particles assumed their original shape whereas high temperature stretched particles did not. (B) Polymer alignment was observed in POM images of 65 °C stretched particles to a higher degree as opposed to 90 °C stretched particles. This indicates that polymer orientation between polymer entanglements maintained in the low-temperature stretched particles, which can serve as driving force to trigger shape memory effect, while disentanglement of polymers happened and polymer orientation were lost in the high-temperature stretched particles.

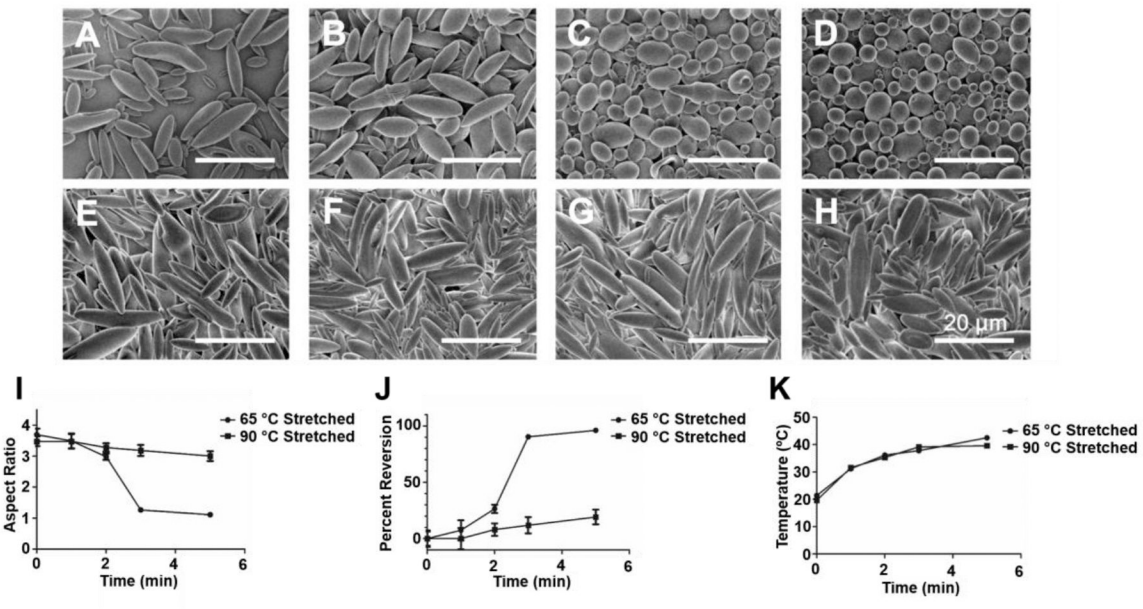

Figure 2.

Thermoplastic shape memory effect can be thermally triggered by light in a temporally controlled fashion. Particles were loaded with hydrophobic gold nanoparticles and stretched at either (A-D) 65 °C or (E-H) 90 °C to generate ellipsoidal microparticles. The particles were then triggered using laser light at 532 nm for (A, E) 1 min, (B, F) 2 min, (C, G) 3 min, or (D, H) 5 min. The particles deformed at 65 °C exhibited full shape reversion to spherical forms whereas the particles stretched at 90 °C did not. (I) Aspect ratio analysis and (J) percent reversion of SEM images demonstrate quantitatively the shape memory effect observed only in particles stretched at 65 °C. (K) The temperature for both 65 °C and 90 °C stretched particle media during laser heating was identical. Error bars represent the standard error of 20 individual particle replicates.

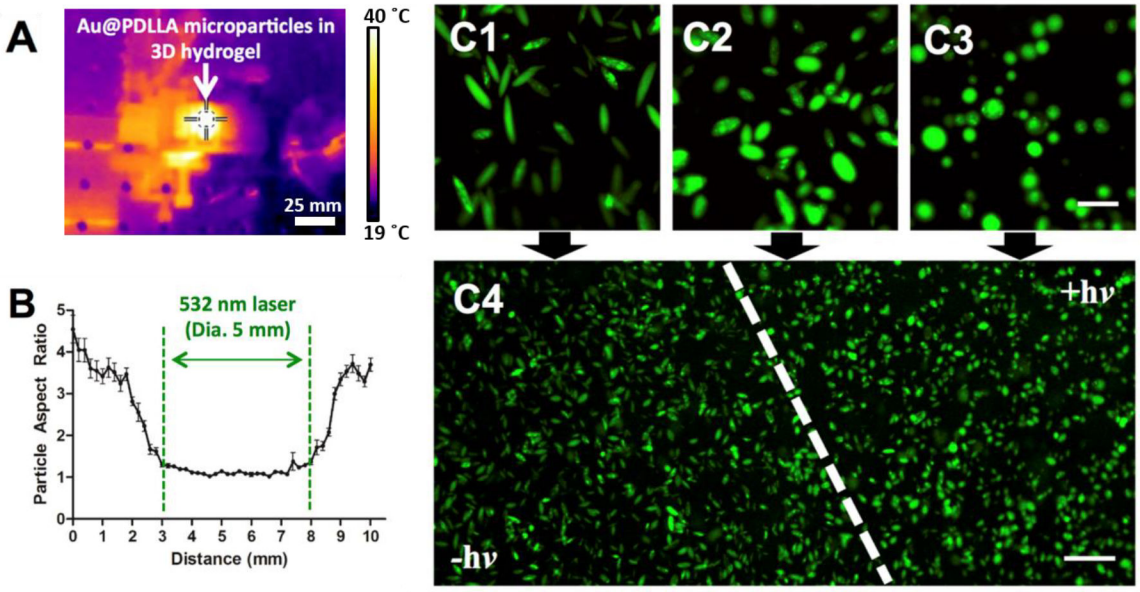

Figure 3.

Shape memory is spatiotemporally controlled by laser irradiation. Ellipsoidal microparticles encapsulating gold nanoparticles were immobilized in a PEG hydrogel and irradiated with a laser at 532 nm. (A) The PEG hydrogel exhibited heating during the laser irradiation process as evidenced by IR imaging. The temperature measured at the center of the crosshairs was 40.0 °C. (B) Particles were subsequently imaged by confocal microscopy and aspect ratio analysis was conducted across the width of the laser irradiation spot. Aspect ratio reversion was detected only within the 5 mm diameter of the laser spot with a 1 mm transition zone on either side. (C) Confocal images of (1) particles not irradiated, (2) particles in transition zone, (3) particles in irradiation zone, (4) zoomed out transition zone illustrate qualitatively the phenomenon illustrated in (B). Error bars represent the standard error of 20 individual particle replicates. Scale bars are 20 μm for images (C1–C3) and 100 μm for image (C4).

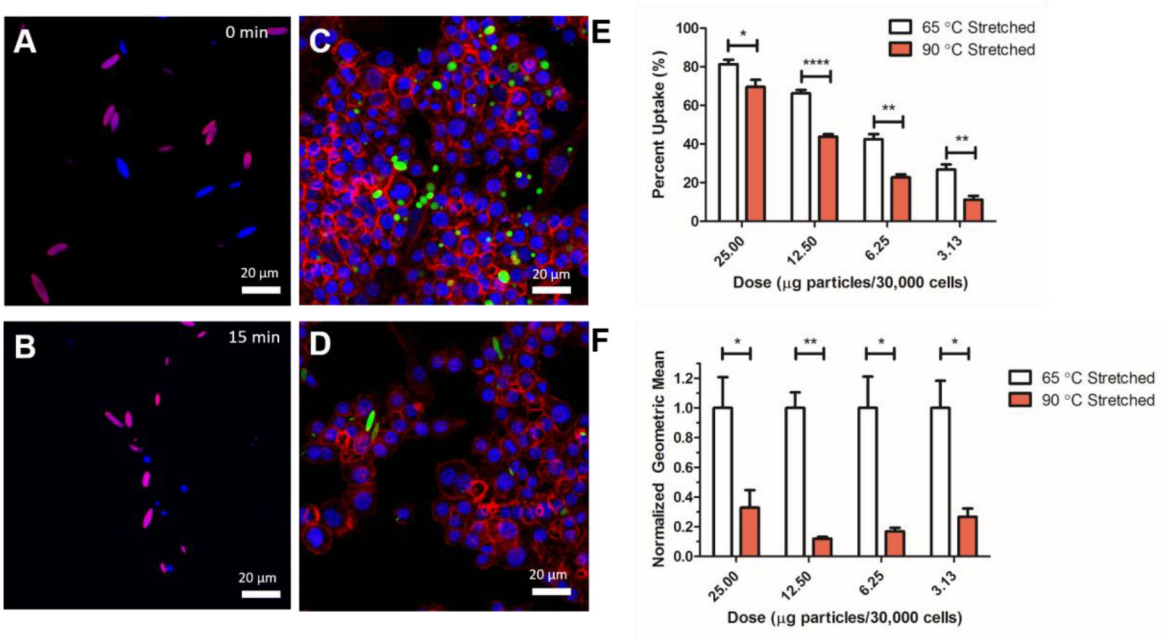

Figure 4.

Phagocytic cells demonstrate different responses to differentially stretched particles that are triggered by the laser. Confocal images of a mixed population of bulk microparticles heated at 45 °C for (A) 0 min and (B) 15 min. For full time course, see Figure S8. 65 °C stretched particles (blue) demonstrate full reversion over the heating whereas 90 °C stretched particles (magenta) demonstrate no reversion to their spherical form. (C) 65 °C stretched and (D) 90 °C stretched particles were cultured with macrophages first heated at 42 °C for 15 min to trigger SME and then incubated at 37 °C for 4 hours. Confocal imaging demonstrates that there is a preference of macrophages to phagocytically take up spherical particles in high quantities compared to non-spherical particles. Blue = DAPI, Red = Actin, Green = Particles. (E) Percent positive uptake and (F) particle fluorescence geometric mean as analyzed by flow cytometry demonstrates that the 65 °C stretched laser triggered shape memory particles were taken up at a higher percentage of the course of 4 hours. Error bars are standard error of n = 4 replicates.